# Enhancing the nonlinear response of plasmonic nanowire antennas by engineering their terminations

Shakeeb Bin Hasan,* Christoph Etrich, Robert Filter, Carsten Rockstuhl, and Falk Lederer
*Institute of Condensed Matter Theory and Solid State Optics, Abbe Center of Photonics, Friedrich-Schiller-Universität Jena, Max-Wien-Platz 1, 07743 Jena, Germany*

(Received 28 May 2013; revised manuscript received 28 August 2013; published 19 November 2013)

Subwavelength light concentration by means of plasmonic nanoantennas is known to significantly enhance the nonlinear response. In nonlinear schemes involving multiple frequencies, however, it remains challenging to design nanoantennas that respond resonantly to more than one or, eventually, to all interacting frequencies. Considering plasmonic nanowire antennas, we hereby demonstrate the potential to engineer their resonances at more than one frequency involved in the nonlinear process by carefully tailoring the antenna terminations. Although we consider here the degenerate nonlinear process of second-harmonic generation, our approach can easily be extended to other nonlinear processes.

DOI: 10.1103/PhysRevB.88.205125 PACS number(s): 42.65.Pc, 73.20.Mf, 42.65.Ky

## I. INTRODUCTION

In recent years, plasmonics has established itself as a promising route towards the nano-scale miniaturization of optical elements.[1] The physical principle which plasmonics is based on is the coupling of electromagnetic radiation to the oscillation of the charge density in noble metals at the metal-dielectric interface.[2] The interest in plasmonics has spurred ever-growing research as well as a body of literature reporting the observation of various optical phenomena in such systems which could be of use in integrated optics and spectroscopic applications, among others. The subwavelength confinement of light leads to a minimization of the geometrical scale where linear effects are observed, which yields a stronger nonlinear interaction due to the high field intensities available in the near field.[3] This triggered investigations into understanding the extent to which strong field localization can beneficially affect the nonlinear process in the face of resistive losses present in metals (for instance, see Refs. 4–9).

In general, the intrinsic and extrinsic nonlinear properties of nano-optical systems can be distinguished.[10] The intrinsic nonlinearity refers to systems where the metals themselves are the sole source of a nonlinear polarization. This makes it possible, for example, to observe a strong third-order nonlinear response. This allows the generation of, e.g., a third harmonic signal upon excitation of optical nanoantennas.[11,12] Alternatively, at the surface of the optical nanoantenna the mirror symmetry of the lattice may be broken and second-order nonlinear effects can be encountered.[13,14] This equally holds when discussing the properties of metals beyond the ordinary Drude model, e.g., the semiclassical hydrodynamic model to describe the dynamics of free electrons,[15–18] or considering quantum-tunneling effects if two plasmonic elements are brought sufficiently close such that electron coupling across the gap results in extreme nonlocality.[19–21] Another interesting mechanism of SH generation in centrosymmetric media is the Lorentzian interaction of electric- and magnetic-field components of the modes.[22] On the contrary, much work has also been studying optical nanosystems with extrinsic nonlinearity.[23,24] The optical nanoantenna's role is to localize light into high near-field intensities, which causes an enhanced nonlinear response from the surrounding nonlinear dielectric medium. Such a case is considered here without any loss of generality.

As a general rule, the nonlinear processes involve the interaction of light oscillating at multiple frequencies depending on the order of nonlinearity and the specific nature of the interaction under consideration. This makes it ideal, if not necessary, to have plasmonic elements that are resonant to all the frequencies involved. Recent studies have attempted to conceive such nanostructures by employing innovative antenna designs that afford tunability at multiple frequencies.[22,25–30] Some of these approaches choose a path where a few individual nanoantennas that sustain resonances at selected frequencies are fused into a single structure. This assures the requirement of having a nanoantenna that sustains resonances at all frequencies of interest.[26–28] In the other approach, the geometrical features of a composite nanoparticle, whether isolated or in array, are tailored to achieve the same end by employing orthogonal polarizations for interacting frequencies.[22,25] In both cases, however, it is challenging to achieve a good spatial overlap—necessary for strong nonlinear response—among the modes at different frequencies which might localize in different arms of the composite antenna geometry. Additionally, the second approach also requires the interacting frequencies to be orthogonally polarized. This can also be a potential drawback when considering that the commonly employed quadratic media exhibit their strongest response through the $d_{33}$ component of their polarizability tensor, which is best utilized if the interacting frequencies are polarized in the same direction. Moreover, it is easy to realize that the fabrication of such structures that consist of multiple elements remains a challenge for current nanofabrication. Even though many top-down as well as bottom-up approaches for nanofabrication are developed, the precise alignment of the individual elements to form the actual nanoantenna constitutes an unnecessary complication. Therefore, it is desirable to have available compact and isolated nanoantennas that can sustain resonances at frequencies on demand.

It is the aim of this paper to explore the potential of cylindrical nanowires as an ideal platform to tailor the

 

nonlinear interaction of light with matter, which meets both aforementioned requirements. Most notably, we show here that with only a single structural entity it is possible to devise nanoantennas that sustain resonances at multiple frequencies which are involved in the nonlinear process. These optical nanowire antennas are superior for various reasons compared to many other nanoantennas. First, their basic functionality is well understood by now, even on the basis of semianalytical models.[31,32] Second, various fabrication methods have been proven to be applicable to realize those nanoantennas with a high precision.[33]

The starting point of the approach to our antenna design is the appreciation that it is not just the length of the nanoantenna that dictates the resonance frequency. Equally the termination of the nanoantenna can provide a significant degree of freedom for tailoring the response of the system. In fact, in limiting cases the termination can even account for the localized resonances exhibited by analytically understood nanoparticles in the quasistatic limit.[34] In these optical nanoantennas a resonance is supported whenever the phase accumulation of a surface plasmon polariton that bounces back and forth in the nanowire experiences a phase accumulation of a multiple of $2\pi$. Contributions to this phase accumulation are due to the propagation along the nanowire, i.e., determined by the dispersion relation, but also by the phase of the complex reflection coefficient. It is essential to stress that both quantities may have a tailored dispersion that can be independently controlled to a large extent. Designing and engineering the nanoantenna termination with the purpose of tailoring the antenna resonances is an often underestimated opportunity. Thus it is only natural to consider the antenna terminations towards an enhancement of multifrequency nonlinear processes as discussed above.

To this end, we combine in our contribution a multitude of theoretical and numerical means to explore the opportunities to tailor the second-order nonlinear response of nanowire antennas embedded in lithium niobate ($LiNbO_3$). Specifically, we utilize an analytical model that can precisely predict the resonances, use a coupled-field theory approach to calculate the strength of the nonlinear response, and verify all our predictions using full-wave simulations that take into account the nonlinear process correctly.

## II. LINEAR PROPERTIES

Figure 1(a) sketches the antenna geometry under consideration. It consists of a cylindrical nanowire of length $L$ that has a semiellipsoidal cap as termination. Two of the three semiaxes of the cap perpendicular to the cylinder's axis are equal to the radius of the nanowire, whereas the third semiaxis, $a$ [Fig. 1(a)], parallel to the cylinder's axis, is allowed to be different. This serves as an additional degree of freedom to tailor the response of the nanoantenna. The limiting case of $a = 0$ would make it an abrupt termination, whereas the limiting case of $L = 0$ would cause the antenna to collapse towards an ellipsoidal nano-particle.[34] When illuminated with a plane wave whose electric field is polarized along the cylinder's axis ($x$ axis) and propagating along the $z$ axis [Fig. 1(a)], a propagating surface plasmon polariton is excited on the nanowire. It bounces back and forth between the semiellipsoidal terminations, where it causes the nanoantenna to sustain eventually Fabry-Perot (FP) resonances at specific frequencies for a fixed geometry. The requirement to observe an antenna resonance at a frequency $\nu$ can be described as[31,33,34]

$$\beta'(\nu)L + \phi_r(a,\nu) = m\pi, \tag{1}$$

where $\beta'(\nu) = \Re\{\beta(\nu)\}$ is the real part of the propagation constant, $\phi_r(a,\nu)$ the phase of the modal reflection coefficient $r(a,\nu)$, $L$ the length of the cavity, and $m$ an integer denoting the order of the FP resonance. The reasoning for the antenna resonance derives from the requirement that the phase accumulation per round-trip shall be a multiple of $2\pi$. It should be pointed out that only symmetric antennas are considered here, i.e., those where the antenna capping is identical for both terminations. Figures 1(b)–1(f) plot the $|E_y|$ field distribution of FP resonances of various order $m$ in the $x$-$z$ cross section of the antenna. It should be noted that unlike odd-order resonances, even-order ones are forbidden by symmetry and were excited by the incoming wave inclined with respect to the $z$ axis on the $x$-$z$ plane [Fig. 1(a)].

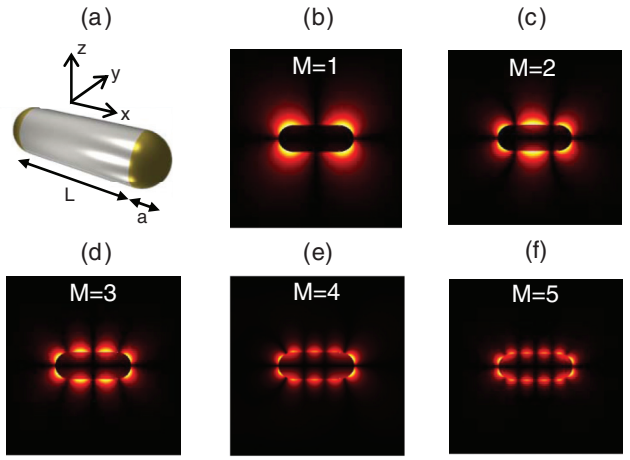


FIG. 1. (Color online) (a) Cylindrical nanowire of length $L$ terminated by semiellipsoidal caps on both sides. Two semiaxes of these caps are shared with the radius of the nanowire, whereas the third axis is a free parameter, labeled $a$. (b)–(f) $|E_y|$ distribution of FP modes of order $M$ when the antenna is illuminated by an $x$-polarized plane wave propagating along the z axis. For exciting modes with even $M$, the exciting wave was inclined with respect to the $z$ axis on the $x$-$z$-plane in order to break the symmetry.

To numerically model the system, we describe the metallic nanoantenna using a Drude fit of Ag[35] defined by the plasma frequency $\omega_p = 1.88 \times 10^3$ THz and damping $\gamma = 19.3$ THz. The surrounding dielectric medium is assumed to be $LiNbO_3$ whose dispersion is isotropically defined, for the sake of computational simplicity, through the extraordinary axis by means of a Sellmeir fit.[36] The anisotropy of the nonlinear $\chi^{(2)}$ tensor, however, is fully considered and its $c$ axis is aligned with the $x$ axis [Fig. 1(a)] to make the most out of the strongest $d_{33}$ coefficient. Since numerical techniques based on the finite-element method (FEM) are more suitable for capturing geometrical curvature,[37] we employed

the commercial FEM-based electromagnetic solver COSMOL MULTIPHYSICS to compute the linear dispersion of the complex modal propagation constant $\beta(\nu)$ of the fundamental $TM_0$ mode on a cylindrical nanowire of 15-nm radius [Fig. 2(a)]. As the radius of the nanowire is sufficiently small compared to the wavelength (quasistatics), we do not need to consider any higher transversal mode supported by the nanowire.[31,34] In order to obtain the modal reflection coefficient from the terminal cap, we employ the computational setup shown in Fig. 2(b). The eigenmode is launched at the $z = 0$ plane where the back-reflection from the antenna termination gets absorbed into the perfectly matched layers (PML) surrounding the computational window. A straightforward application of the orthogonality relation established through the unconjugated reciprocity theorem[38] leads to the following equation for the modal reflection coefficient:

$$r(a,\nu) = -\exp(-i2\beta' l)\frac{\int_0^\infty E_{\rho,0}(\rho,\nu)[H_\phi(\rho,z=0,a,\nu) - H_{\phi,0}(\rho,\nu)]\rho\, d\rho}{\int_0^\infty E_{\rho,0}(\rho,\nu)H_{\phi,0}(\rho,\nu)\rho\, d\rho}. \quad (2)$$

$E_{\rho,0}(\rho,\nu)$ and $H_{\phi,0}(\rho,\nu)$ denote the radially and azimuthally polarized electric- and magnetic-field components of the eigenmode supported by an infinitely extended nanowire, respectively. Likewise, $H_\phi(\rho,z,a,\nu)$ denotes the total magnetic field within the computational domain that introduces the dependence upon the cap radius $a$. The length $l$ of the antenna in Fig. 3(b) was chosen large enough so as to remove any dependence of $r(a,\nu)$ on it due to coupling to higher order evanescent modes, although the application of orthogonality relations should already have significantly suppressed it. At the $z = 0$ plane, $H_\phi(\rho,z=0,a,\nu)$ is a superposition of incident and reflected modes from which the contribution of the incident eigenmode is subtracted to obtain the reflection coefficient. Figures 2(c) and 2(d) display the squared amplitude $R = |r(a,\nu)|^2$ and phase $\phi_r(a,\nu) = \arg[r(a,\nu)]$ of the dispersive modal reflection coefficient.

Given the strong dispersion of $r(a,\nu)$ [Figs. 2(c) and 2(d)] upon both the frequency and the cap geometry, we attempt to explore the possibility of aligning FP resonances of different orders with the frequencies taking part in the nonlinear process. To this end, we propose to exploit the semiaxis $a$ of the cap as a degree of freedom in design parameters while keeping the radius of the nanowire constant. This can be desirable in circumstances where strong field localization is required because the fundamental $TM_0$ mode shows increasing localization with decreasing wire radius.[34] As for the specific nonlinear interaction considered, we choose to work with the degenerate nonlinear process of (SH) generation when the metallic cylinder is embedded in a dielectric medium possessing a $\chi^{(2)}$ response. More complex scenarios involving three- or four-wave mixing (cubic media) can be explored along the same lines.

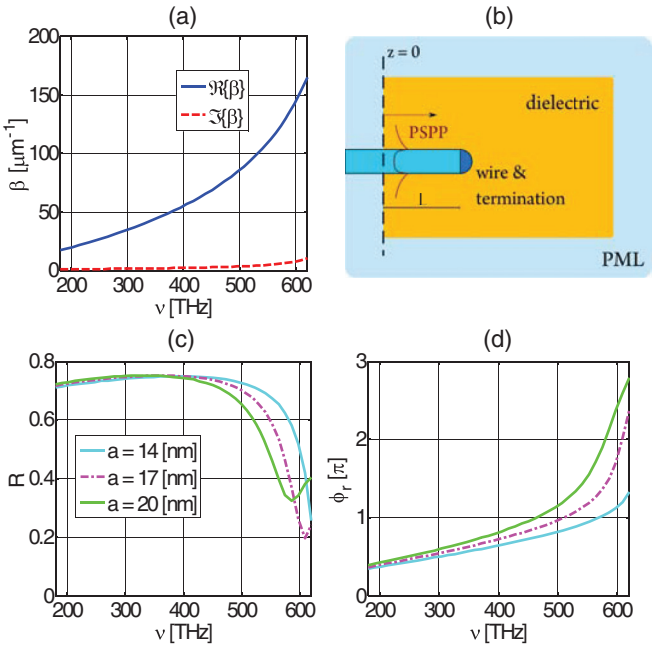


FIG. 2. (Color online) (a) Dispersion of fundamental $TM_0$ mode computed for a cylindrical wire of radius 15 nm. (b) Schematic of the three-dimensional geometry used to obtain the modal reflection coefficient $r(a,\nu)$ of the $TM_0$ mode. (c) Squared amplitude $R(a,\nu) = |r(a,\nu)|^2$ (c) and phase $\phi_r(a,\nu) = \arg[r(a,\nu)]$ (d) of the reflection coefficient.

## III. NONLINEAR PROPERTIES

From the linear simulations we can extract all the information necessary to predict the spectral position of the FP resonances of the antenna. In terms of the antenna length $L$,

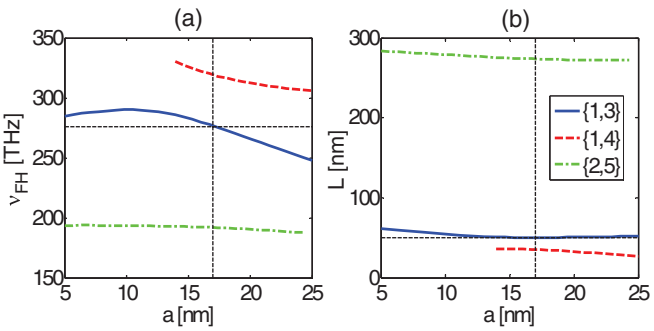


FIG. 3. (Color online) (a) Pump frequency $\nu_{FH}$ and (b) length $L$ for the given cap radius $a$ where double resonance is possible for FP orders $m$ and $n$ at FH and SH, respectively. Horizontal and vertical black lines indicate the operating configuration ($\nu$ = 276 THz, $a$ = 17 nm, and $L$ = 50 nm) chosen in this study.

the resonance condition of Eq. (1) can be written as

$$L_m = \frac{m\pi - \phi_r(a,\nu_{FH})}{\beta'(\nu_{FH})}, \quad L_n = \frac{n\pi - \phi_r(a,2\nu_{FH})}{\beta'(2\nu_{FH})},$$

where $m$ and $n$ are integers denoting the order of the FP resonances at FH and SH frequencies, respectively. In order to find configurations with a resonant response at both the fundamental harmonic (FH) and the corresponding SH, we solve for the condition $L_m = L_n$. Figure 3 displays the result when the semiaxis $a$ is varied from 5 to 25 nm and the FH frequency from 180 to 320 THz. The figures have to be read such that for a desired operation frequency of the FH a certain semi-axis $a$ can be derived [cf. Fig. 3(a)]. Using this specific $a$ the corresponding antenna length $L$ can be read off from Figs. 3(a) and 3(b), such that the corresponding antenna sustains a resonance at both the FH and the SH frequencies. Allowing for different FP orders at FH and SH, we obtained doubly resonant configurations for the combination of firstorder at FH with third and fourth order at SH, and the combination of second order at FH with fifth order at SH, as indicated in the figure. It can be seen that a suitable design that covers the entire frequency spectrum is not found for the present rather restrictive geometry. However, for quite a large spectral domain in multiple intervals double-resonant nanoantennas can be perceived.

Considering only the bright resonances, i.e., excitable resonances, under normal illumination [parallel to the $z$ axis; Fig. 1(a)], we work exclusively with the scheme exhibiting first- and third-order resonances at FH and SH frequency, respectively, in Fig. 3. However, this is by no means a general restriction because the other combinations could have been explored as well.

In order to compare the predicted resonance frequencies to those supported by the actual structure, first we performed linear full-wave simulations. Specifically, we considered an array of antennas arranged in a periodic lattice of 200 × 200 nm in the transverse $x$-$y$ plane. The period was chosen large enough such that the interaction among neighboring nanoantennas may be disregarded. Choosing a test case of $a = 17$ nm, we find $L = 50$ nm and $\nu_{FH} = 277$ THz as the configuration for double resonance from Fig. 3. The periodic array is excited with $x$-polarized light according to Fig. 1(a) to compute the linear response of the system. Figures 4(a) and 4(c) show the transmission results when the cap semiaxis $a$ and the length $L$ of the antenna are detuned. A detailed inspection clearly demonstrates the double-resonance characteristic at both FH and SH in the fully resonant case. It can be extracted from the figure that the resonances predicted with the analytical model are indeed supported by the structure at the correct frequencies.

To theoretically understand the advantage of doubly resonant antennas for nonlinear interactions, in the second step we take advantage of the undepleted pump approximation to describe the nonlinear interaction of the near fields at both the FH and the SH frequency.[39] Accordingly, the strength of the nonlinear interaction is described in terms of an effective nonlinear coefficient $\gamma$ which depends crucially on the field

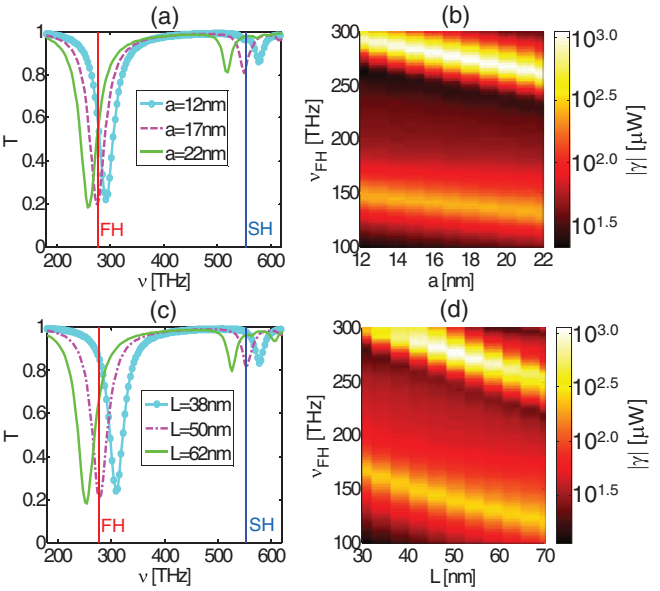


FIG. 4. (Color online) (a) Linear transmission spectrum and (b) nonlinear mode overlap $|\gamma|$ for cap detuning. (c) Linear transmission and (d) mode overlap when the length of the antenna is detuned. The nonlinear mode overlap is obtained by illuminating with a pump of power 1 W per unit cell. Please note that $|\gamma|$ is shown on a logarithmic scale.

overlap and is defined under Kleinman's symmetry as

$$\gamma \approx \varepsilon_0 \nu_{FH} \iiint d_{33}(\mathbf{r}) E_x^2(\mathbf{r},\nu_{FH}) E_{sx}^{\star}(\mathbf{r},2\nu_{FH}) d\mathbf{r}, \quad (3)$$

where $E_x(x,y,\nu)$ is the $x$ component of the total FH field (incident plane wave and scattered field by the periodic array), while $E_{sx}(\mathbf{r},\nu)$ denotes the $x$ component of the scattered (without excitation at the SH frequency) SH field. Equation (3) is approximately written in terms of the dominant $d_{33}$ coefficient of the contracted $\chi^{(2)}$ tensor, which is at least one order of magnitude stronger than the rest.[36] In numerical simulations, however, the full anisotropic $\chi^{(2)}$ tensor is taken into account.

By illuminating the periodic array with a plane wave of power 1 W per unit cell, we scanned for the variation of $|\gamma|$ in the case of cap and length detuning as before. The results are shown in Figs. 4(b) and 4(d). We find an enhancement in $|\gamma|$ by approximately twice the order of magnitude when $\nu_{FH} = 277$ THz and the cap axis $a = 17$ nm [Fig. 4(b)] or length $L = 50$ nm [Fig. 4(b)]. Another bright line is also visible when the incident pump frequency is $\nu_{FH} = 139$ THz. This happens because the corresponding SH frequency coincides with the first-order FP resonance of the antenna and the nonlinear response is equally enhanced in such a single-resonant configuration although less pronounced.

To corroborate the predicted enhancement in nonlinear interaction, we performed nonlinear full-wave simulations using our in-house code based on the finite-difference time-domain (FDTD) method. The grid size in the discretized space was chosen to be 1 nm, whereas metallic and dielectric dispersion was incorporated through the fits described earlier.

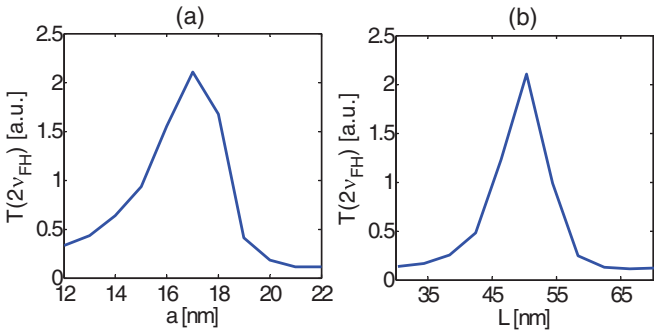


FIG. 5. (Color online) (a) Transmission spectrum of nonlinear FDTD simulations when illuminated with a continuous-wave pump of power 13 mW at $\nu = 277$ THz showing the effect of detuning (a) the cap radius $a$ where $L = 50$ nm and (b) the length $L$ where $a = 17$ nm from their resonant values of $a = 17$ nm and $L = 50$ nm, respectively.

The instantaneous nonlinear response of the dielectric medium was incorporated into the FDTD simulation as[40]

$$\mathbf{P}^{(2)}(\mathbf{r},t) = 2\varepsilon_0 \begin{pmatrix} d_{33}(\mathbf{r})E_x(\mathbf{r},t)^2 + d_{31}(\mathbf{r})E_y(\mathbf{r},t)^2 \\ 2d_{31}(\mathbf{r})E_x(\mathbf{r},t)E_y(\mathbf{r},t) \\ 0 \end{pmatrix}. \quad (4)$$

For the sake of computational simplicity, we omitted in our code [hence Eq. (4)] those components of the contracted $\chi^{(2)}$ tensor which introduce dependence on the $E_z$ field, which is negligibly smaller than the others. Illuminating the periodic array with a continuous-wave pump at $\nu_{FH} = 277$ THz and carrying 13 mW power per unit cell, we computed the power flux in transmission at SH through a periodic cell. Figures 5(a) and 5(b) show the results for the two specific cases of cap and length detuning discussed earlier, respectively. An order-of-magnitude enhancement is observed in the generated SH when the geometrical parameters coincide with the doubly resonant configuration [Figs. 4(a) and 4(c)], clearly demonstrating the advantage of our scheme.

The scenarios discussed so far, however, do not fully distinguish the merit of having doubly resonant antennas. Therefore, we calculated the antenna configuration when illuminated at the same frequency ($\nu_{FH} = 277$ THz) but with the geometrical parameters varied to keep only one of the two resonances at pump or SH frequency as shown in Fig. 6(a). To clarify the role of the resonance at SH, we chose to work on the red line in Fig. 6(a), which describes the geometrical configuration where the antenna is always resonant at $\nu_{FH} = 277$ THz. It is clearly seen that the SH is only resonant for a specific, the doubly resonant, configuration. Only if this configuration is met is a double-resonant scheme achieved; otherwise, the nanoantenna is only singly resonant at FH.

Figure 6(b) shows the corresponding results for linear transmission simulation performed in the same manner as discussed earlier in the context of Fig. 4. We find the FH to be always resonant at $\nu_{FH} = 277$ THz as enforced but the SH is detuned except when the cap semiaxis is $a = 17$ nm. Figure 6(c) scans the value of $|\gamma|$. The bright line in Fig. 6(c) at $\nu_{FH} = 139$ THz shows no geometrical dependence because

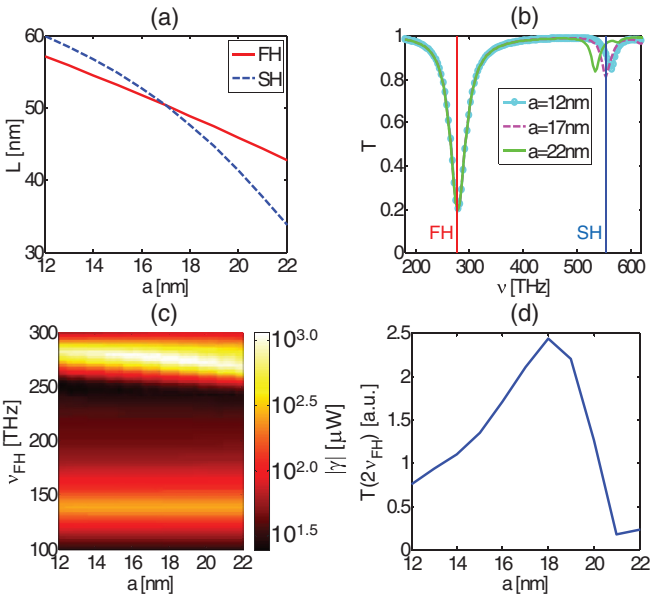


FIG. 6. (Color online) (a) Antenna configuration at $\nu_{FH} = 277$ THz when the FH has an FP resonance of first order and an SH of third order. (b) Linear transmission spectrum and (c) nonlinear mode overlap $|\gamma|$ when the antenna is kept resonant at FH according to (a). (d) Transmission spectrum of nonlinear FDTD simulations when the structure is illuminated with a pump of $\nu_{FH} = 277$ THz.

the antenna is always resonant at the corresponding SH. But the bright line around $\nu_{FH} = 277$ THz is slanted, indicating a prominent dependence upon the SH resonance of the antenna, which keeps changing for different geometrical configurations. Figure 6(d) shows the computed SH transmission spectrum in nonlinear FDTD simulations whose computational details are the same as described earlier. The peak for the largest SH signal is reached in Fig. 6(c) for $a = 18$ nm, which is close enough to the predicted value of $a = 17$ nm. This minor deviation can be attributed to disparity between the numerical methods: the FEM for the analytical prediction and the FDTD method for nonlinear computations. However, overall we see an excellent agreement and a clear demonstration of the positive impact doubly resonant antennas can have on enhancing the efficiency of nonlinear interactions.

## IV. CONCLUSION

In conclusion, we have proposed and numerically demonstrated that a simple plasmonic antenna consisting of a cylindrical metallic nanowire with semiellipsoidal terminations provides sufficient degrees of freedom such that it can be tuned to have double resonance sustained across an extended range of incident frequencies. Through rigorous linear and nonlinear full-wave FDTD simulations, the superiority of doubly resonant structures over singly resonant ones has been demonstrated for the specific case of SH generation. The key that unlocked these tuning opportunities was the appreciation that the terminations of the nanoantennas, i.e., their cappings, can be independently controlled from the main body of the nanoantenna, i.e., the wire. This degree of freedom has thus far not been exploited in the context of nonlinear

plasmoncics. Although fabrication of the suggested structures sounds challenging, currently available high-resolution top-down nanofabrication techniques, e.g., based on helium-ion lithography, can be used in perspective. Alternatively, bottom-up approaches can also be used, e.g., based on the controlled reduction of a metal salt on an existing nanowire for homogeneous material systems,[41] but also for heterogenous material systems[42] if desired. Our findings have the potential to greatly enhance the outcome of more complex, nondegenerate parametric interactions, leading to novel applications in optical spectroscopy and computing.

## ACKNOWLEDGMENTS

Support from the German Federal Ministry of Education and Research (PhoNa), the Thuringian State Government (MeMa), and the German Science Foundation (SPP 1391 Ultrafast Nano-optics) is acknowledged.

*shakeeb-bin.hasan@uni-jena.de

[1] D. K. Gramotnev and S. I. Bozhevolnyi, Nat. Photon. **4**, 83 (2010).
[2] S. A. Maier, *Plasmonics: Fundamentals and Applications* (Springer, Berlin, 2007).
[3] M. Kauranen and A. V. Zayats, Nat. Photon. **6**, 737 (2012).
[4] K. D. Ko, A. Kumar, K. H. Fung, R. Ambekar, G. L. Liu, N. X. Fang, and K. C. Toussaint, Nano Lett. **11**, 61 (2011).
[5] M. Ren, E. Plum, J. Xu, and N. I. Zheludev, Nat. Commun. **3**, 833 (2012).
[6] G. Hajisalem, A. Ahmed, Y. Pang, and R. Gordon, Opt. Express. **20**, 29923 (2012).
[7] S. Linden, F. B. P. Niesler, J. Förstner, Y. Grynko, T. Meier, and M. Wegener, Phys. Rev. Lett. **109**, 015502 (2012).
[8] S. B. Hasan, C. Rockstuhl, T. Pertsch, and F. Lederer, J. Opt. Soc. Am. B **29**, 1606 (2012).
[9] A. R. Davoyan, I. V. Shadrivov, and Y. S. Kivshar, Opt. Express. **17**, 21732 (2009).
[10] T. Utikal, T. Zentgraf, T. Paul, C. Rockstuhl, F. Lederer, M. Lippitz, and H. Giessen, Phys. Rev. Lett. **106**, 133901 (2011).
[11] J. Reinhold, M. R. Shcherbakov, A. Chipouline, V. I. Panov, C. Helgert, T. Paul, C. Rockstuhl, F. Lederer, E.-B. Kley, A. Tünnermann *et al*., Phys. Rev. B **86**, 115401 (2012).
[12] M. Hentschel, T. Utikal, H. Giessen, and M. Lippitz, Nano Lett. **12**, 3778 (2012).
[13] A. Slablab, L. L. Xuan, M. Zielinski, Y. de Wilde, V. Jacques, D. Chauvat, and J.-F. Roch, Opt. Express. **20**, 220 (2012).
[14] J. Butet, I. Russier-Antoine, C. Jonin, N. Lascoux, E. Benichou, and P.-F. Brevet, J. Opt. Soc. Am. B **29**, 2213 (2012).
[15] C. Ciraci, E. Poutrina, M. Scalora, and D. R. Smith, Phys. Rev. B **86**, 115451 (2012).
[16] C. Ciraci, E. Poutrina, M. Scalora, and D. R. Smith, Phys. Rev. B **85**, 201403(R) (2012).
[17] P. Ginzburg, A. Krasavin, Y. Sonnefraud, A. Murphy, R. J. Pollard, S. A. Maier, and A. V. Zayats, Phys. Rev. B **86**, 085422 (2012).
[18] T. Paul, C. Rockstuhl, and F. Lederer, J. Mod. Opt. **58**, 438 (2011).
[19] K. J. Savage, M. M. Hawkeye, R. Esteban, A. G. Borisov, J. Aizpurua, and J. J. Baumberg, Nature **491**, 574 (2012).
[20] J. A. Scholl, A. Garcia-Etxarri, A. L. Koh, and J. A. Dionne, Nano Lett. **13**, 564 (2013).
[21] R. Esteban, A. G. Borisov, P. Nordlander, and J. Aizpurua, Nat. Commun. **3**, 825 (2012).
[22] B. Z. Steinberg, Opt. Express. **19**, 25843 (2011).
[23] C. Argyropoulos, P.-Y. Chen, G. D'Aguanno, N. Engheta, and A. Alù, Phys. Rev. B **85**, 045129 (2012).
[24] P.-Y. Chen and A. Alu, Nano Lett. **11**, 5514 (2011).
[25] U. K. Chettiar and N. Engheta, Phys. Rev. B **86**, 075405 (2012).
[26] H. Harutyunyan, G. Volpe, R. Quidant, and L. Novotny, Phys. Rev. Lett. **108**, 217403 (2012).
[27] M. Abb, Y. Wang, P. Albella, C. H. de Groot, J. Aizpurua, and O. L. Muskens, ACS Nano **6**, 6462 (2012).
[28] K. Thyagarajan, S. Rivier, A. Lovera, and O. J. Martin, Opt. Express **20**, 12860 (2012).
[29] H. Aouani, M. Navarro-Cia, M. Rahmani, T. P. H. Sidiropoulos, M. Hong, R. F. Oulton, and S. A. Maier, Nano Lett. **12**, 4997 (2012).
[30] A. Hänsel, O. A. Egorov, S. B. Hasan, C. Rockstuhl, and F. Lederer, Phys. Rev. A **85**, 053843 (2012).
[31] L. Novotny, Phys. Rev. Lett. **98**, 266802 (2007).
[32] R. Gordon, Opt. Express **17**, 18621 (2009).
[33] J. Dörfmuller, R. Vogelgesang, R. T. Weitz, C. Rockstuhl, C. Etrich, T. Pertsch, F. Lederer, and K. Kern, Nano Lett. **9**, 2372 (2009).
[34] S. B. Hasan, R. Filter, A. Ahmed, R. Vogelgesang, R. Gordon, C. Rockstuhl, and F. Lederer, Phys. Rev. B **84**, 195405 (2011).
[35] P. B. Johnson and R. W. Christy, Phys. Rev. B **6**, 4370 (1972).
[36] http://www.lambdaphoto.co.uk/pdfs/Inrad_datasheet_LNB.pdf
[37] C. Hafner and J. Smajic, J. Mod. Opt. **58**, 467 (2011).
[38] J. L. A. W. Snyder, *Optical Waveguide Theory* (Springer, Berlin, 1984).
[39] A. Hayat and M. Orenstein, Opt. Lett. **32**, 2864 (2007).
[40] R. W. Boyd, *Nonlinear Optics*, 3rd ed. (Academic Press, New York, 2008).
[41] E. Carbó-Argibay, B. Rodríguez-González, J. Pacifico, I. Pastoriza-Santos, J. Pérez-Juste, and L. M. Liz-Marzán, Angew. Chem. **119**, 9141 (2007).
[42] A. Sánchez-Iglesias, E. Carbó-Argibay, A. Glaria, B. Rodríguez-González, J. Pérez-Juste, I. Pastoriza-Santos, and L. M. Liz-Marzán, Chem. Eur. J. **16**, 5558 (2010).